CCI+ PHASE 2 – NEW ECVS
PERMAFROST

CCN4 OPTION 7
IceInSAR: INFERRED ACTIVE LAYER WATER/ICE CONTENT AND FREEZE-THAW PROGRESSION FROM ASSIMILATING InSAR IN PERMAFROST MODEL

D3.2 CLIMATE RESEARCH DATA PACKAGE (CRDP)

VERSION 1.0

30 SEPTEMBER 2024

PREPARED BY

Document Status Sheet

Issue	Date	Details	Authors
1.0	30.09.2024	First version	LW, LR, SW, AB, TS

Author team

Lotte Wendt and Line Rouyet, NORCE

Sebastian Westermann, UiO

Annett Bartsch, B.GEOS

Tazio Strozzi, GAMMA

ESA Technical Officer

Frank Martin Seifert

Table of contents

Executive summary

Within the European Space Agency (ESA), the Climate Change Initiative (CCI) is a global monitoring program which aims to provide long-term satellite-based products to serve the climate modelling and climate user community. The two main products associated to the ECV Permafrost are Ground Temperature (GT) and Active Layer Thickness (ALT). GT and ALT are documented by the Permafrost_cci project based on thermal remote sensing and physical modelling.

The Permafrost_cci models take advantage of additional datasets, such as snow cover and land cover, to estimate the heat transfer between the surface and the underground. However, several challenges remain due to spatially variable subsurface conditions, especially in relation to unknown amounts of water/ice in the active layer that modify the effective heat capacity and the thermal conductivity of the ground. In complex terrain with large spatial heterogeneities, coarse and partly inadequate land cover categorisation, the current results show discrepancies with in-situ measurements, which highlight the need to assimilate new data sources as model input. Although the ground stratigraphy is not directly observable from space, it impacts the dynamics of the ground surface. The seasonal thawing and refreezing induce cyclic subsidence and heave of the ground surface due to ice formation and melt in the active layer, and can therefore be used as indirect indicator of the ground conditions.

Synthetic Aperture Radar Interferometry (InSAR) based on Sentinel-1 images can be used to measure the amplitude and seasonal progression of these displacements. The movement amplitude is related to the amount of water/ice that is affected by a phase change, whilst the timing of the displacement patterns reflects the vertical progression of the thawing/freezing front. Considering the fine to medium spatial resolution of Sentinel-1 images, InSAR time series therefore have the potential to enhance the characterisation of subsurface hydrogeologic and thermal parameters and adapt the existing Permafrost_cci models to improve their performance at the local to regional scale. The *IceInSAR* pilot project (Option 7) will develop a prototype for permafrost model adjustment by assimilating Sentinel-1 InSAR surface displacement maps and time series into the model to constrain stratigraphy parameters. *IceInSAR* will provide pilot products, expected to be used for adjustment of the ECV processing chain of the baseline project in a next phase.

This Climate Research Data Package (CRDP) presents the results generated as part of the *IceInSAR* Option 7. The document describes the Option 7 datasets, which are further compared and discussed in the associated Product Validation and Intercomparison Report (PVIR) [RD-1] and the Product User Guide (PUG) [RD-2]. The CRDP has been published on ZENODO:

Wendt, L. (2024). Ground ice contents and InSAR displacements from Adventdalen, Svalbard. [Data set]. Zenodo. https://doi.org/10.5281/zenodo.11187360.

1   Introduction

1.1   Purpose of the document

This document summarizes the data produced in the *IceInSAR* Option 7. It has to be read together with the PVIR [RD-1] and the PUG [RD-2].

1.2   Structure of the document

Section 2 introduces the study design. Section 3 describes the in-situ data. Section 4 describes the InSAR data. Section 5 described the model outputs. Section 6 summarizes the conclusions and prospects. Section 7 includes a bibliography and list of acronyms. A glossary of the commonly accepted permafrost terminology can be found in RD-15.

1.3   Applicable Documents

[AD-1] ESA. 2022. Climate Change Initiative Extension (CCI+) Phase 2 – New Essential Climate Variables – Statement of Work. ESA-EOP-SC-AMT-2021-27.

[AD-2] GCOS. 2022. The 2022 GCOS Implementation Plan. GCOS – 244 / GOOS – 272. Global Observing Climate System (GCOS). World Meteorological Organization (WMO).

[AD-3] GCOS. 2022. The 2022 GCOS ECVs Requirements. GCOS – 245. Global Climate Observing System (GCOS). World Meteorological Organization (WMO).

1.4   Reference Documents

[RD-1] Wendt, L., Rouyet, L., Westermann, S., Bartsch, A., Strozzi, T. 2024. ESA CCI+ Permafrost Phase 2. CCN4 Option 7. IceInSAR: Inferred Active Layer Water/Ice Content and Freeze-Thaw Progression From Assimilating InSAR in Permafrost Model. D.4.1 Product Validation and Intercomparison Report (PVIR). Version 1.0. European Space Agency.

[RD-2] Wendt, L., Rouyet, L., Westermann, S., Bartsch, A., Strozzi, T. 2024. ESA CCI+ Permafrost Phase 2. CCN4 Option 7. IceInSAR: Inferred Active Layer Water/Ice Content and Freeze-Thaw Progression From Assimilating InSAR in Permafrost Model. D.4.2 Product User Guide (PUG). Version 1.0. European Space Agency.

[RD-3] Rouyet, L., Wendt, L., Westermann, S., Bartsch, A., Strozzi, T. 2023. ESA CCI+ Permafrost Phase 2. CCN4 Option 7. IceInSAR: Inferred Active Layer Water/Ice Content and Freeze-Thaw Progression From Assimilating InSAR in Permafrost Model. D.1.1 User Requirement Document (URD). Version 1.0. European Space Agency.

[RD-4] Rouyet, L., Wendt, L., Westermann, S., Bartsch, A., Strozzi, T. 2023. ESA CCI+ Permafrost Phase 2. CCN4 Option 7. IceInSAR: Inferred Active Layer Water/Ice Content and Freeze-Thaw Progression From Assimilating InSAR in Permafrost Model. D.1.2 Product Specification Document (PSD). Version 1.0. European Space Agency.

[RD-5] Rouyet, L., Wendt, L., Westermann, S., Bartsch, A., Strozzi, T. 2023. ESA CCI+ Permafrost Phase 2. CCN4 Option 7. IceInSAR: Inferred Active Layer Water/Ice Content and Freeze-Thaw Progression From Assimilating InSAR in Permafrost Model. D.2.2 Algorithm Theoretical Basis Document (ATBD). Version 1.0. European Space Agency.

[RD-6] Rouyet, L., Wendt, L., Westermann, S., Bartsch, A., Strozzi, T. 2023. ESA CCI+ Permafrost Phase 2. CCN4 Option 7. IceInSAR: Inferred Active Layer Water/Ice Content and Freeze-Thaw Progression From Assimilating InSAR in Permafrost Model. D.2.3 End-to-End ECV Uncertainty Budget (E3UB). Version 1.0. European Space Agency.

[RD-7] Rouyet, L., Wendt, L., Westermann, S., Bartsch, A., Strozzi, T. 2023. ESA CCI+ Permafrost Phase 2. CCN4 Option 7. IceInSAR: Inferred Active Layer Water/Ice Content and Freeze-Thaw Progression From Assimilating InSAR in Permafrost Model. D.2.4 Algorithm Development Plan (ADP). Version 1.0. European Space Agency.

[RD-8] Rouyet, L., Wendt, L., Westermann, S., Bartsch, A., Strozzi, T. 2023. ESA CCI+ Permafrost Phase 2. CCN4 Option 7. IceInSAR: Inferred Active Layer Water/Ice Content and Freeze-Thaw Progression From Assimilating InSAR in Permafrost Model. D.2.5 Product Validation Plan (PVP). Version 1.0. European Space Agency.

[RD-9] Bartsch, A., Matthes, H., Westermann, S., Heim, B., Pellet, C., Onaca, A., Strozzi, T., Kroisleitner, C., Strozzi, T. 2023. ESA CCI+ Permafrost Phase 2. D.1.1 User Requirement Document (URD). Version 3.0. European Space Agency.

[RD-10] Bartsch, A., Westermann, S., Strozzi, T., Wiesmann, A., Kroisleitner, C., Wieczorek, M., Heim, B. 2023. ESA CCI+ Permafrost Phase 2. D.1.2 Product Specification Document (PSD). Version 3.0. European Space Agency.

[RD-11] Westermann, S., Bartsch, A., Strozzi, T. 2023. ESA CCI+ Permafrost. D.2.2 Algorithm Theoretical Basis Document (ATBD). Version 4.0. European Space Agency.

[RD-12] Westermann, S., Bartsch, A., Strozzi, T. 2023. ESA CCI+ Permafrost. D.3.2 Climate Research Data Package (CRDP). Version 4.0. European Space Agency.

[RD-13] Bartsch, A., Obu, J., Westermann, S., Strozzi, T. 2024. ESA CCI+ Permafrost. D.4.3 Product User Guide (PUG). Version 4.1. European Space Agency.

[RD-14] Heim, B., Wieczorek, M., Pellet, C., Delaloye, R., Bartsch, A., Strozzi, T. 2024. ESA CCI+ Permafrost. D.4.1 Product Validation and Intercomparison Report (PVIR). Version 4.0. European Space Agency.

[RD-15] van Everdingen, Robert, Ed. 1998 revised May 2005. Multi-language glossary of permafrost and related ground-ice terms. Boulder, CO: National Snow and Ice Data Center/World Data Center for Glaciology (http://nsidc.org/fgdc/glossary/; accessed 23.09.2009).

1.5   Bibliography

A complete bibliographic list that supports arguments or statements made within the current document is provided in Section 7.1.

1.6   Acronyms

A list of acronyms is provided in Section 7.2.

2 Proof-of-concept study design

The *IceInSAR* Option 7 is a proof-of-concept study. The primary objective is to evidence the value of Interferometric Synthetic Aperture Radar (InSAR) surface displacement to indirectly document the ground stratigraphy, and elaborate strategies for data assimilation into permafrost models.

To fulfil this objective, a significant focus has been placed on comparing InSAR displacement with in-situ data acquired in Adventdalen, Svalbard (see PVIR [RD-1]) (Wendt, 2024a). An extensive field dataset on the subsurface stratigraphies and permafrost ECV variables was acquired in spring-autumn 2023 (see Section 3). Due to the timing of this field campaign, most InSAR analyses have been performed for the 2023 snow-free season (see Section 4.1). The CRDP is stored on Zenodo (Wendt, 2024b), and is further described in the PUG [RD-2].

In addition to the 2023 results, seasonal InSAR displacement time series have been processed for all other available Sentinel-1 seasons, using both ascending and descending SAR orbits (see Section 4.2). Interannual displacement time series have also been generated (see Section 4.3). These datasets are not published yet, as this part of the Option 7 is in synergy with the parallel project developing an InSAR Ground Motion Service in Svalbard (Rouyet et al., 2024). The data release is planned for end of 2025 and will be made openly available for viewing and download in a WebGIS similar to the InSAR Norway service (https://insar.ngu.no/). The InSAR products served as basis for experiments to further elaborate data assimilation strategies into permafrost models (e.g. InSAR clustering) (see Section 4.4).

Simulations with the CryoGrid community permafrost model (Westermann et al., 2023) were performed at selected locations where both in-situ and InSAR data were available (see Section 5). These simulations make it possible to benchmark various model schemes and parametrizations against in-situ and remotely sensed observations, with the objective to develop processing chains that can ingest InSAR data into permafrost models. The code is open and accessible in GitHub repository (https://github.com/CryoGrid/CryoGridCommunity_run).

In the following, we present 1) the in-situ ground ice and thaw depth data (Section 3), 2) the InSAR displacement data (Section 4), and 3) the CryoGrid model outputs (Section 5). The results of the comparison between InSAR and in-situ data, as well as between InSAR data and model outputs are further discussed in the PVIR [RD-1].

3 In-situ data

A field campaign supported by an Arctic Field Grant (Norwegian Research Council, project no. 342203, RiS ID 12143) was carried out in spring–autumn 2023. The in-situ data collection aimed to verify how the InSAR displacement relates to the subsurface stratigraphy and ground ice distribution. In April–May 2023, sediment cores of the active layer and the uppermost permafrost (depth: 0.63–2.02 m) were extracted at 12 coring sites (Figure 1) and a large set of geocryological parameters were retrieved from laboratory analysis (stratigraphy, organic content, ground ice content, dominating lithology and texture). In September 2023, thaw depth was probed surrounding the coring sites. The details of the procedure are explained in Wendt (2024a). Uncertainties associated to these measurements are described in the PVIR [RD-1].
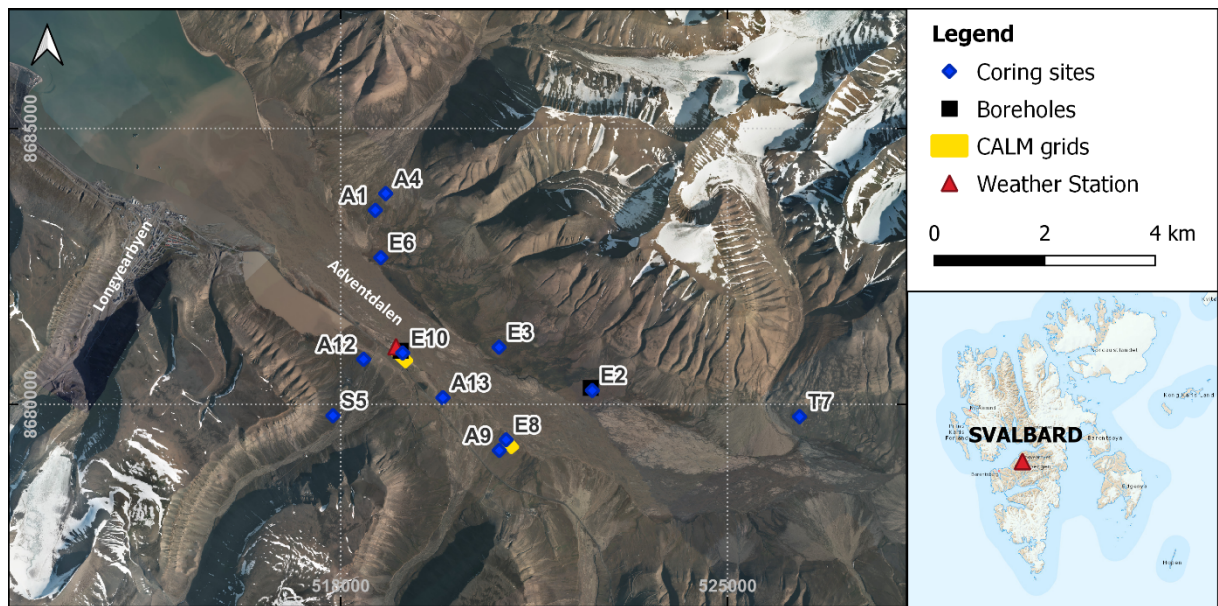
Figure 1: Location map with coring sites and other reference measurement stations. From Wendt (2024a).

The results show a large variety of ground conditions, which confirm that the dataset is well-suited to test the assumptions of Option 7. The Volumetric Ice Content (VIC) and Excess Ice Content (EIC) clearly differ depending on the core grain size (Figure 2). VIC and EIC vary with depth, showing generally ice-rich conditions in the upper active layer and the uppermost permafrost and relatively ice-poor central sections (Figure 3). Based on the measured ice contents, expected subsidence from pore ice and/or excess ice was calculated at each site. The total expected subsidence (τ) is calculated as followed:

$$\tau = \sum_0^{ALT}(pore\ ice\ melt\ +\ excess\ ice\ melt\ +\ excess\ ice\ meltwater\ drainage) \times l_c$$

$$\tau = \sum_0^{ALT}(0.08 \times \text{PIC} + 0.08 \times EIC + 0.92 \times EIC) \times l_c$$

where PIC = VIC – EIC, and l_c = the core length.

The equation is based on established consensus regarding the volume loss of different ice components (Morgenstern and Nixon, 1971; Farouki, 1981; Van Everdingen, 1998). The detailed explanations about the calculation can be found in Wendt (2024a).
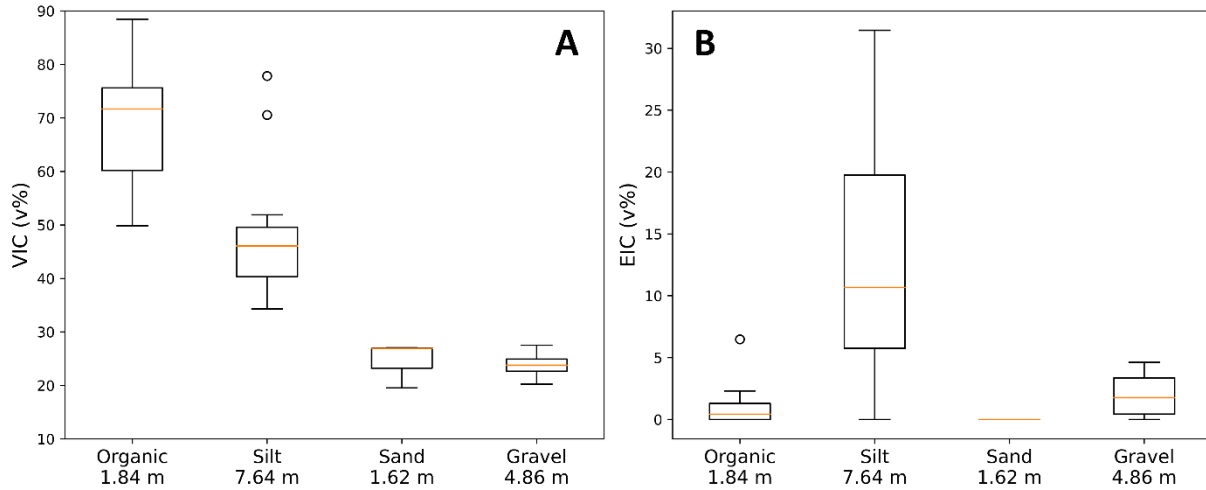
Figure 2: A. Volumetric Ice Content (VIC). B. Excess Ice Content (EIC). The results are categorized by grain size type, based on the 12 coring sites. The value below each grain size label is the cumulated length of the core sections used for each boxplot. From Wendt (2024a).
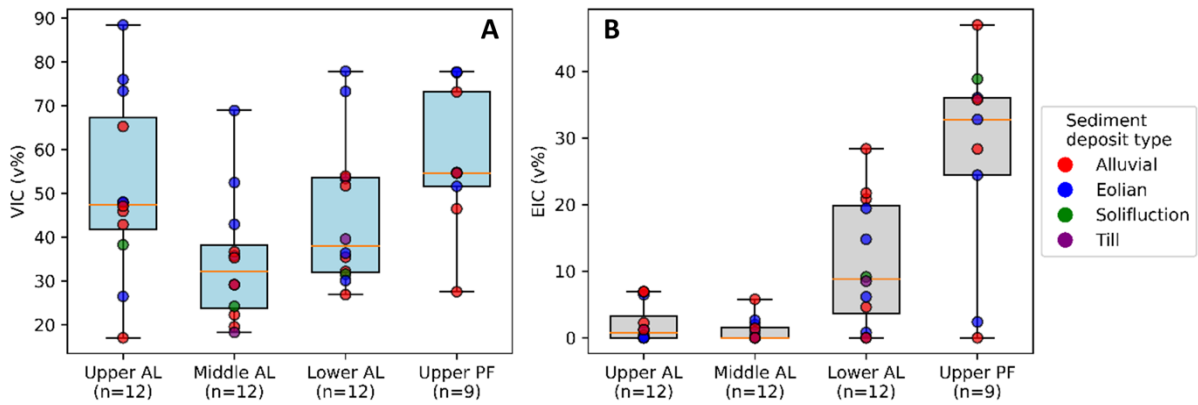
Figure 3: A. Volumetric Ice Content (VIC). B. Excess Ice Content (EIC). The results are categorized by depth locations (upper, centre and lower thirds of the active layer and the uppermost permafrost), based on the 12 coring sites. From Wendt (2024a).

The probed thaw depths and inferred Active Layer Thickness (ALT) values from all sites were compared with the expected subsidence τ (Figure 4). ALT is moderately correlated with the expected subsidence from pore ice melt. The correlation is negative: the lower the subsidence values, the larger the ALT (Figure 4A). There is no correlation between the ALT and the expected subsidence from excess ice melt (including water drainage) (Figure 4B). As a result of the dominant contribution from excess ice melt and drainage, the ALT is not correlated with the total expected subsidence τ (Figure 4C).
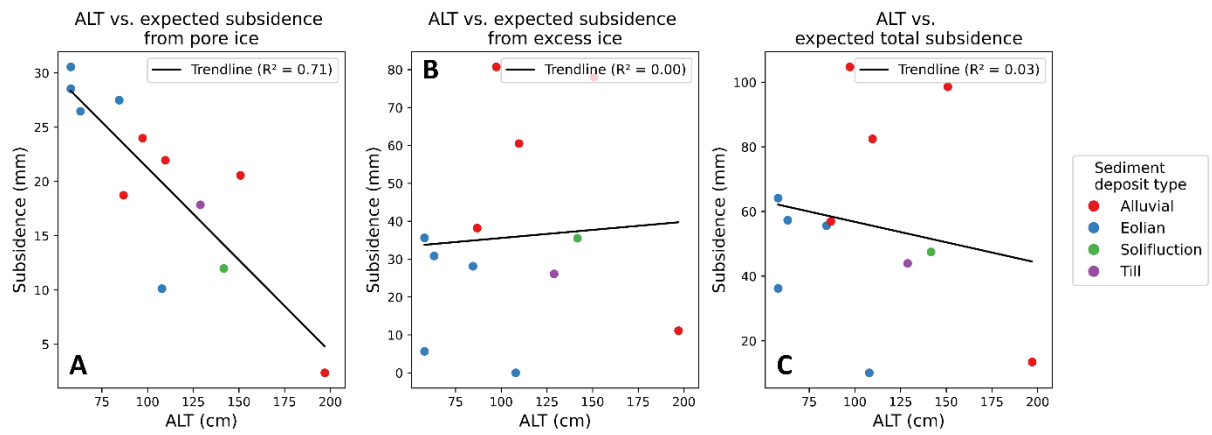
Figure 4: Relationship between the Active Layer Thickness (ALT) and the expected subsidence from pore ice and/or excess ice melt within the active layer. From Wendt (2024a).

4 InSAR data

4.1 Seasonal InSAR displacement in 2023

Seasonal displacement time series were processed with a Small Baseline Subset (SBAS) InSAR algorithm following the procedure described in the ATBD [RD-5]. Sentinel-1 SAR acquisitions are available over Svalbard every 6 to 12 days, depending on the season. In 2023, due to failure of Sentinel-1B in 2021, acquisitions were only available every 12 days. A total of 13 interferograms generated from images acquired with a descending orbit were used to generate May–September displacement time series. Ascending results were also generated but one missing acquisition led to decreased quality (see PVIR [RD-1]). A wide range of maximal seasonal displacement is detected in the flat lowland terrain, which aligns with the variety of the sediment deposit types across the valley (Figure 5). The distribution shows similar patterns as previously published InSAR results in the area (Rouyet et al., 2019; 2021).
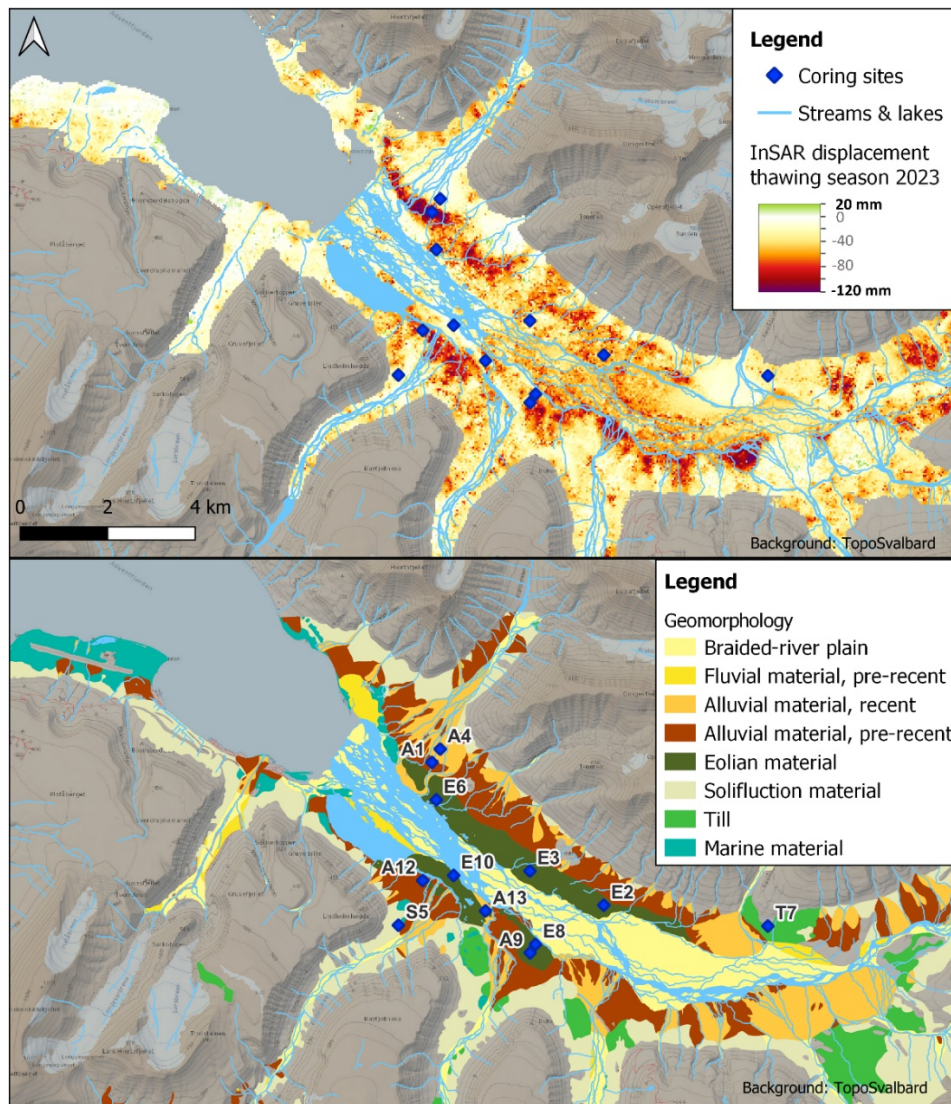
Figure 5: Upper: Seasonal maximal vertical InSAR displacement during the thawing season 2023. Negative values indicate subsidence. Positive value indicate uplift. Lower: Sediment deposit types based on Härtel & Christiansen (2014). From Wendt (2024a).

At the location of the field sites, the SBAS InSAR displacement time series were extracted (Figure 6). The time series spans the snow-free thawing period in the area. Both the subsidence patterns and subsidence magnitude vary depending on the location, which indicates that the locations represent a wide variety of conditions, valuable for the Option 7 proof-of-concept study.
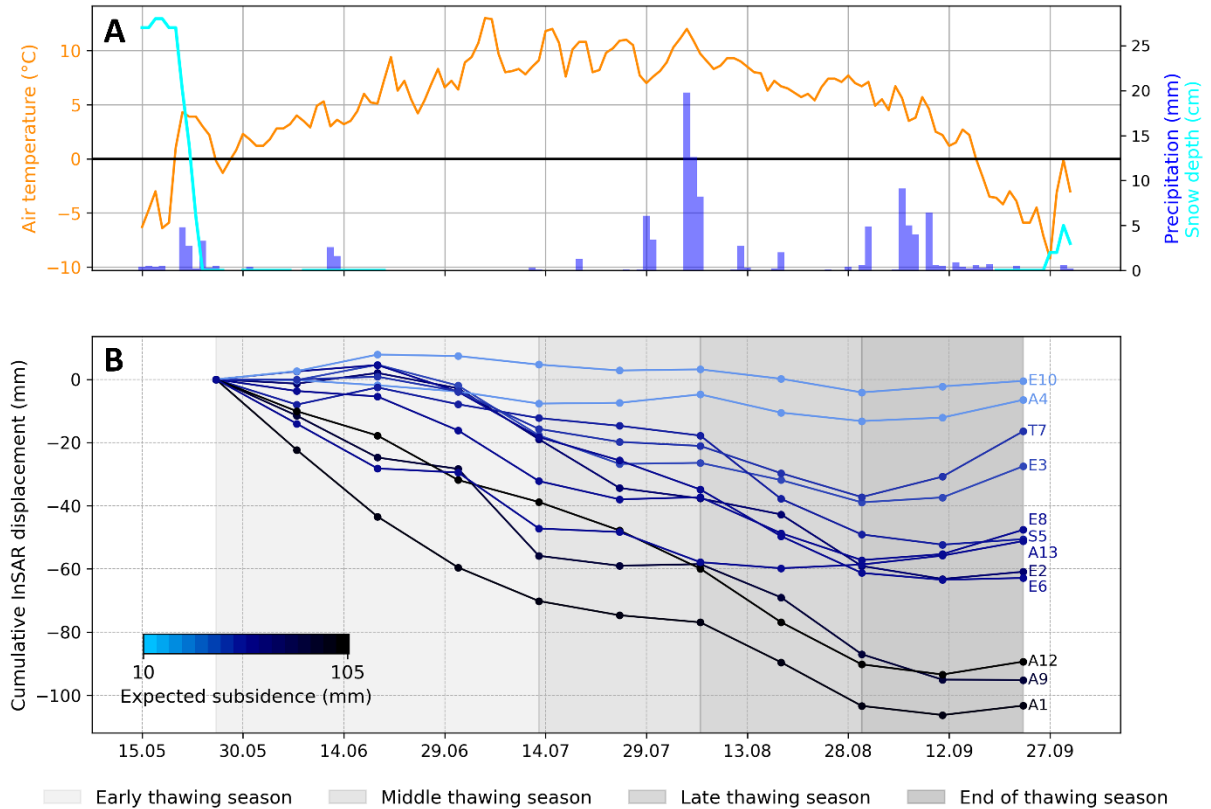
Figure 6: A. Meteorological data between May and September 2023. B. Seasonal InSAR displacement time series at the field sites (location: blue dots in Figures 1 and 5). From Wendt (2024a).

4.2   Seasonal InSAR displacement in 2016–2022

Other seasons (2016–2022) were similarly processed using both ascending and descending data, when available (Figure 7). Similar SBAS processing was performed around Ny-Ålesund, Svalbard (Figure 8). However, due to the acquisition of field data in 2023 (see Section 3), further analysis and comparison with in-situ data and modelling results focuses on 2023 InSAR data in Adventdalen.
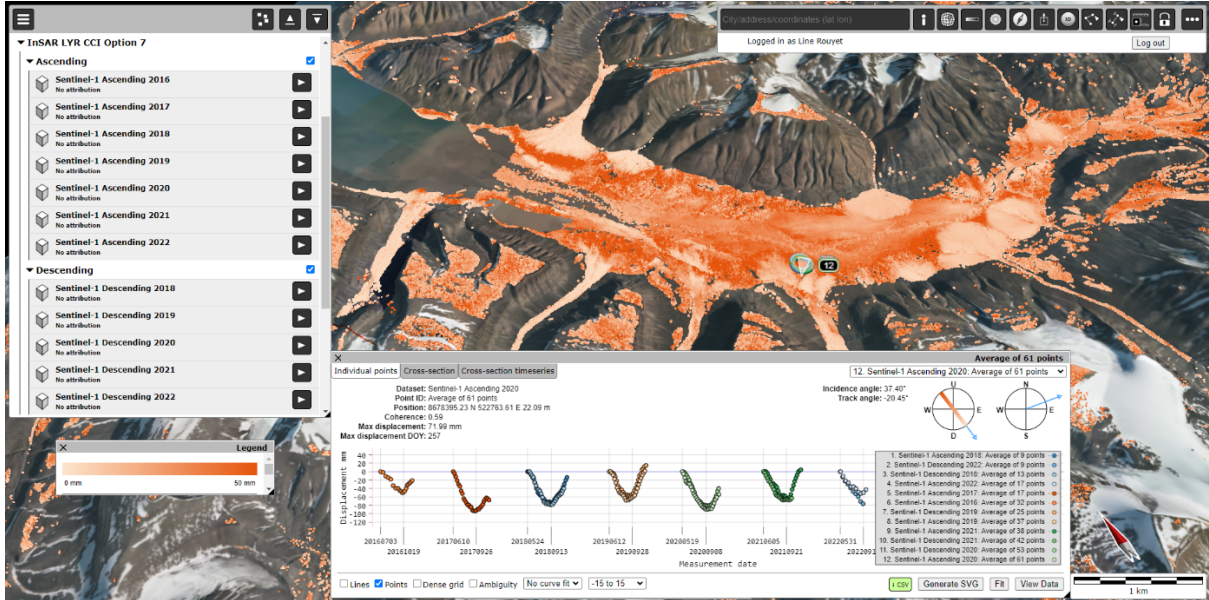
Figure 7: Overview of the processed 2016–2022 seasonal InSAR time series in Adventdalen, visualized in the NORCE NLIVE WebGIS tool.
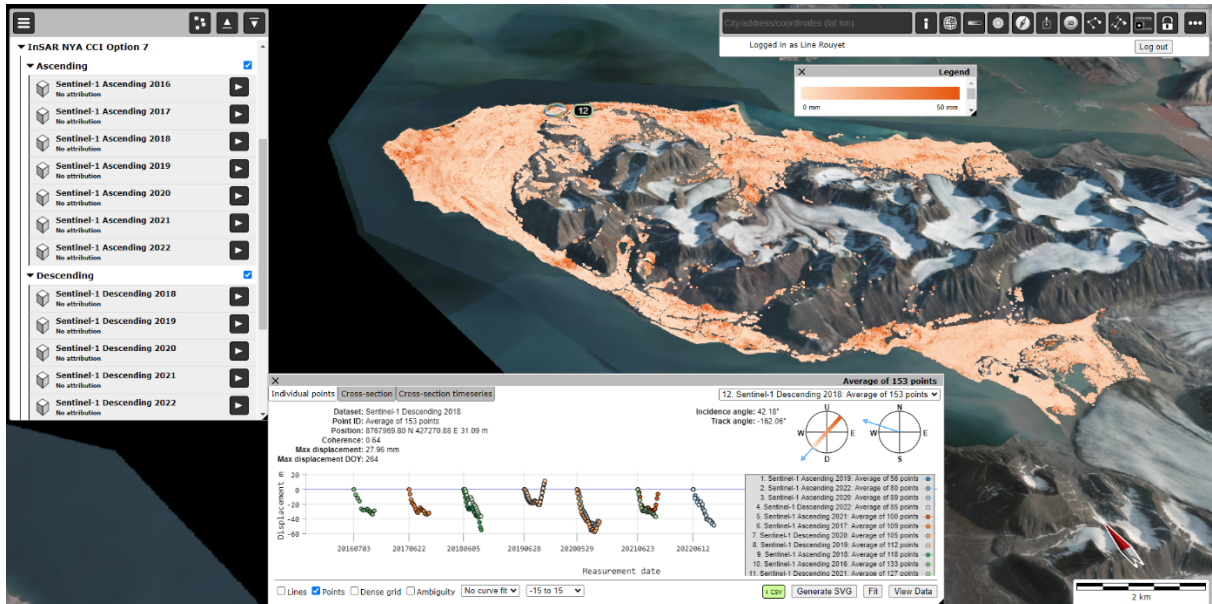
Figure 8: Overview of the processed 2016–2022 seasonal InSAR time series around Ny-Ålesund, visualized in the NORCE NLIVE WebGIS tool.

4.3   Interannual InSAR displacement

Annual interferograms (340–390d temporal baselines; descending orbit) were generated between May and September 2018–2023. In total 118 were selected to generate an interannual InSAR time series, documenting the long-term ground surface movement. The measurement coverage decreases compared to the seasonal products (Figure 5) due to lower interferometric coherence. However, clear spatial patterns are still visible and align with the amplitude of the seasonal patterns. This fits the assumption that areas with an ice-rich active layer are likely more vulnerable to long-term subsidence due to ice-rich transient layer and upper permafrost. Further discussion of the interannual results can be found in Wendt (2024a). The results were combined with seasonal displacement times series from Section 4.1 to generate a simplified clustered InSAR map (see Section 4.4).
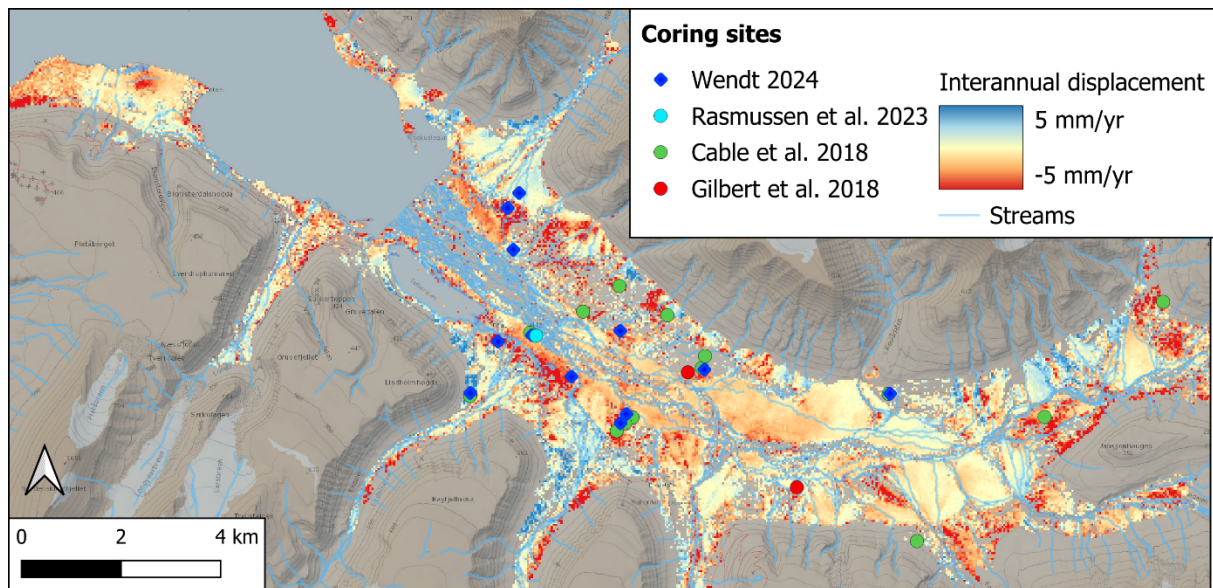
Figure 9: Map of the interannual displacement trend (mm/year) in Adventdalen. Modified from Wendt, 2024a. The comparison with field data from past studies (Rasmussen et al., 2023; Cable et al., 2018; Gilbert et al., 2018) is further discussed in Wendt (2024a).

4.4   Clustered InSAR map

With the objective to develop simplified products practically suited for data assimilation in CryoGrid, a clustering experiment was performed. A k-means clustering technique was applied based on two attributes: the seasonal InSAR displacement time series in 2023 and the 2018–2023 interannual displacement trend. The resulting map consists of five classes with contrasting displacement patterns (Figure 6A), which provides a well-suited simplified product summarizing the behaviour of the ground surface, in relation with the upper subsurface composition. It should be noted that the areas affected by large seasonal movement are overall also those displaying a larger interannual subsiding trend (Figure 6B and 6C), which indicate that both seasonal and interannual time series are good indicators of the relative distribution of the excess ice-rich vs ice-poor conditions in the upper ground. This is a first promising experiment that should be complemented by future tests with different seasons and/or in different regions.
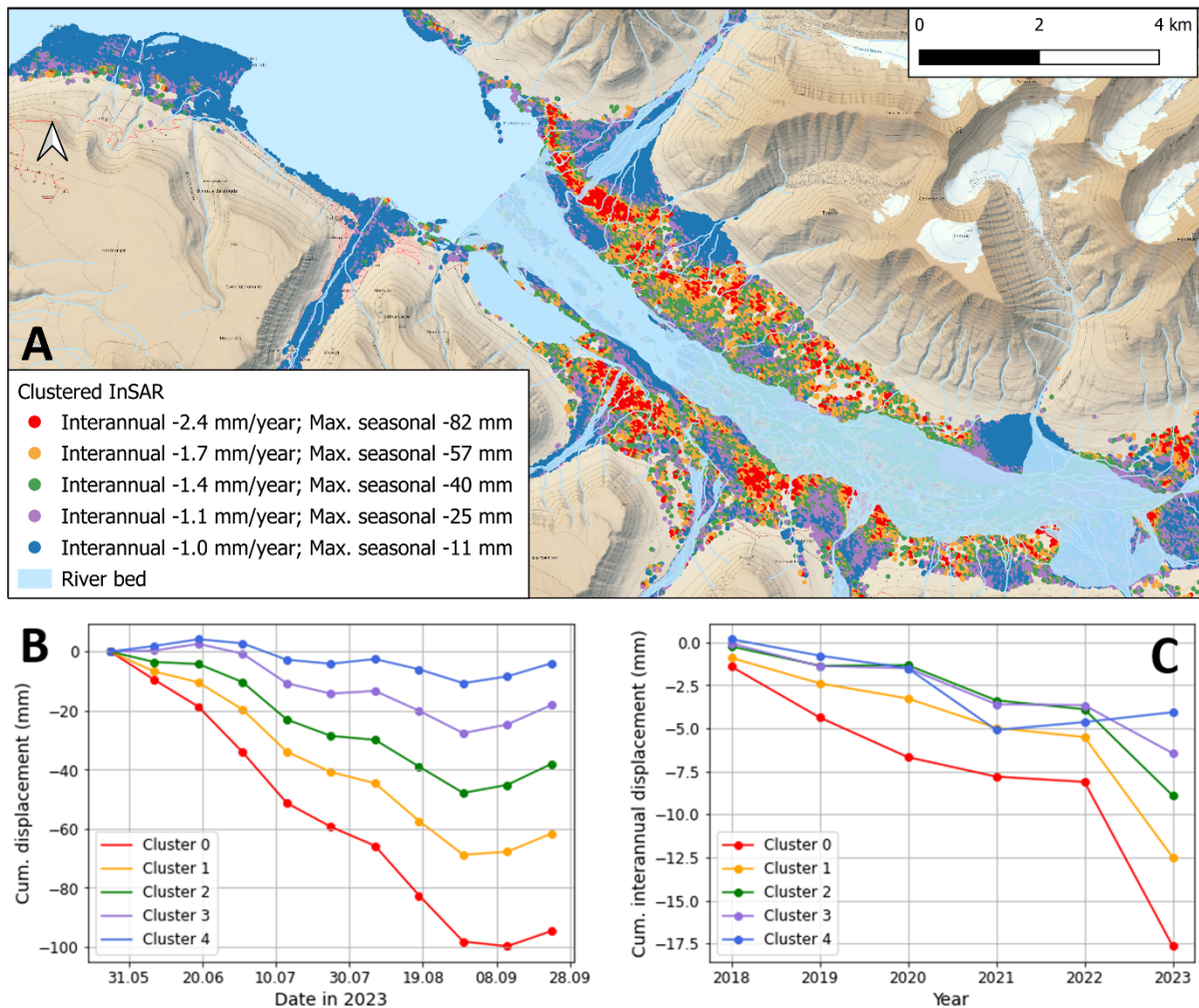
Figure 10: A. Clustered InSAR map generated using k-means clustering the documented pixels based on two attributes: the seasonal InSAR displacement time series and the interannual displacement trends. B. The 2023 mean seasonal InSAR timeseries per cluster. C. The 2018–2023 mean interannual InSAR timeseries per cluster. Modified from Wendt (2024a).

5   Model outputs

To evaluate the potential of assimilating InSAR data into the permafrost model CryoGrid, model simulations were performed at two sites. The simulated ice content changes and resulting simulated surface displacements of the CryoGrid model were compared with the InSAR displacements.

To capture the variability of subsurface conditions in the study area, we selected two sites with contrasting conditions according to the in-situ data: site E10 (dry loess site with little excess ice) and site E2 (wet organic site with abundant excess ice) (locations in Figure 1). The properties of these sites are detailed in Wendt (2024a).

The simulations were performed using the CryoGrid community model (Westermann et al., 2023) and focussed on the annual ground temperature and soil moisture dynamics, including the seasonal thaw progression and evolution of ground ice distribution. The performance of two model configurations was tested against in-situ observations: 1) the pore ice configuration, including only formation/melt of pore ice, but neglecting formation and melt of excess ice, and 2) the segregation ice configuration, considering the formation/melt of both pore and excess ice. The first configuration closely resembles the setup used for Permafrost_cci product generation. The second model configuration is based on the prototype developed by Aga et al. (2023). Details of the model parametrization are described in Wendt (2024a).

The simulated ground ice contents of the pore ice model at the dry site (E10) and the wet site (E2) are respectively shown in Figure 11 and Figure 12. At the dry site, the pore ice model captures very well the ground ice conditions observed in-situ (Figure 11). At the wet site, the volumetric ice content also aligns with the in-situ measurements (Figure 12). However, since no excess ice can form in this configuration, all of the volumetric ice content is present within the model soil pore space. This model configuration does not allow for simulating soil column expansion and compression from excess ice formation and melt.
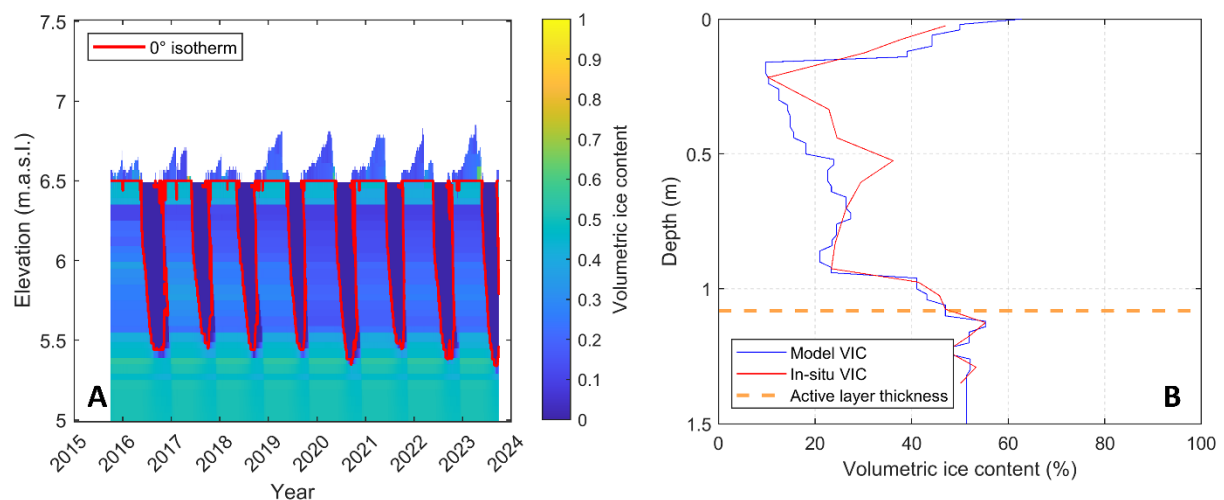
Figure 11: A. Modelled ground ice dynamics from pore ice model at the dry site (E10). B. Comparison between modelled and measured VIC (26.04.2023). Modified from Wendt (2024a).
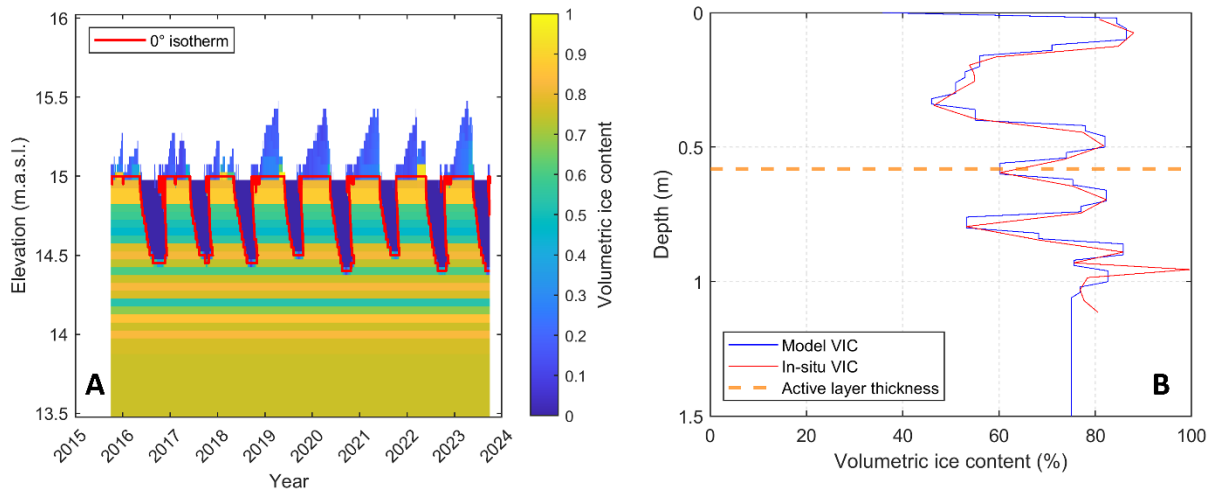
Figure 12: A. Modelled ground ice dynamics from pore ice model at the wet site (E2). B. Comparison between modelled and measured VIC (17.04.2023). From Wendt (2024a).

The segregation ice model configuration can simulate both the pore ice and the excess ice contents. In this case, the volumetric ice content is the summation of the pore ice and the ice excess content. This model configuration allows for simulating soil column expansion and compression from excess ice formation and melt. The simulated ground ice contents for the wet site (E2) are shown Figure 13. A detailed view of the results for 2023 is shown in Figure 14.
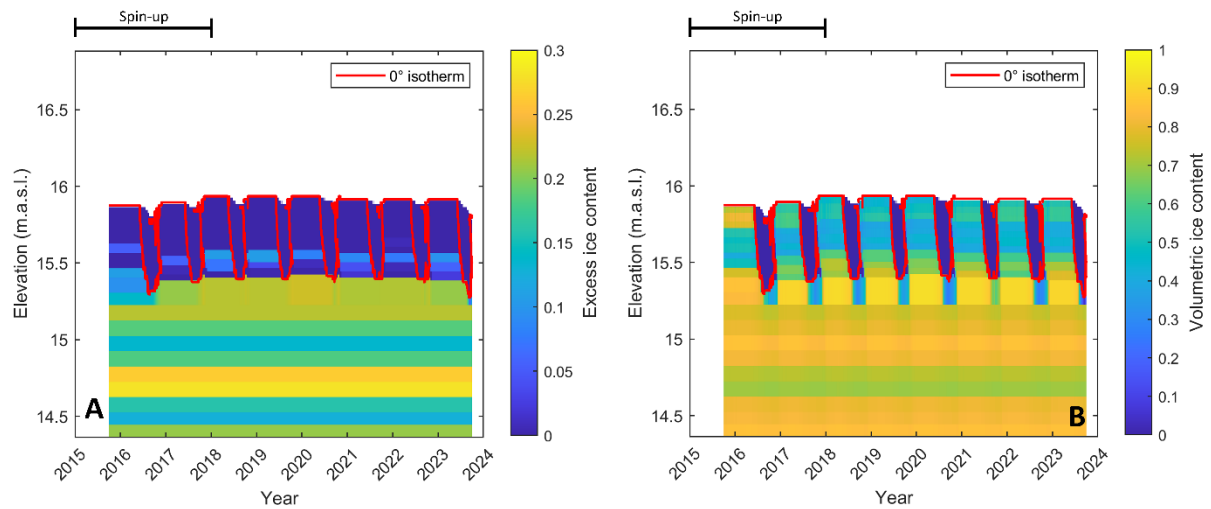
Figure 13: A. Modelled Excess Ice Content dynamics at the wet site (E2). B. Modelled Volumetric Ice Content dynamics at the wet site (E2). From Wendt (2024a).
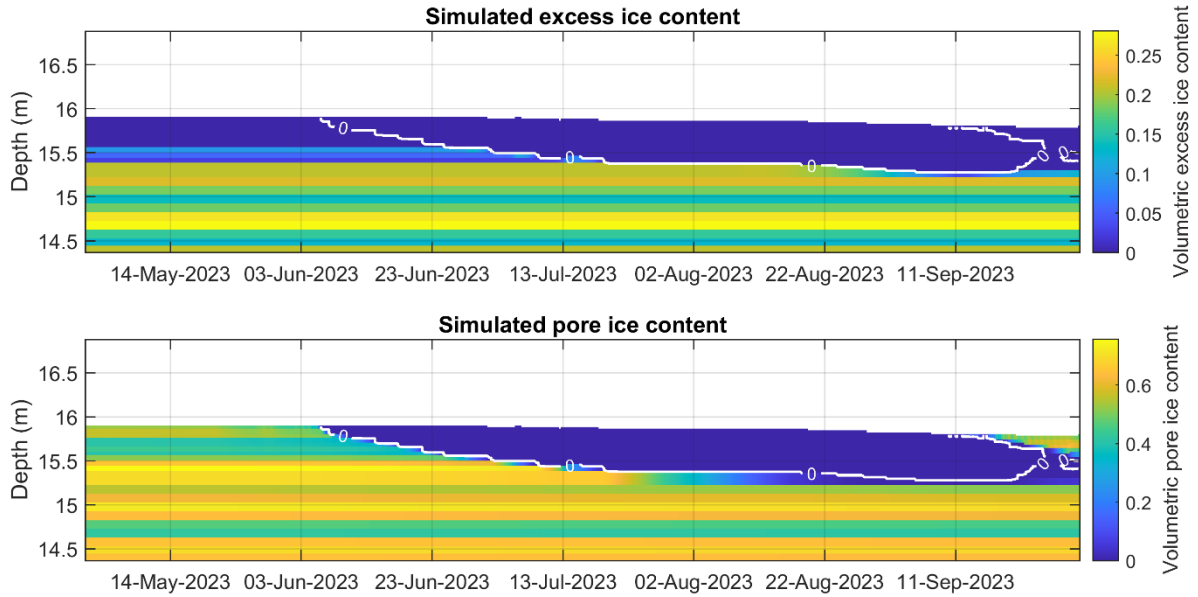
Figure 14: Detailed simulation results for 2023: modelled excess ice content (upper) and pore ice content (lower) using the segregation ice model configuration. From Wendt (2024a).

The two different model configurations simulate similar surface subsidence time series at the dry site (E10), where there is little excess ice (Figure 15A). Using the pore ice model, the simulated surface subsidence time series match the InSAR displacements at the dry site, indicating a high potential of assimilating InSAR products for model calibration. However, at the wet site (E2), the pore ice model fails to reproduce the observations (Figure 15B). The results clearly improve when using the segregation ice model. When considering the contribution of excess ice, the simulated subsidence matches well the InSAR displacement time series (Figure 16).
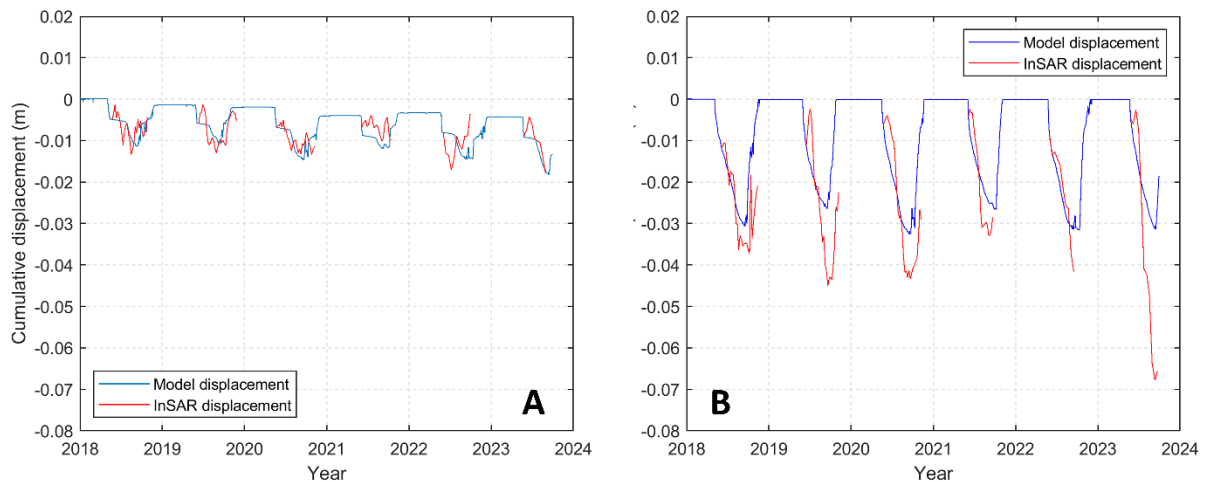
Figure 15: Simulations of the pore ice model. A. Simulated displacement time series compared to InSAR observations at the dry site (E10) B. Simulated displacement time series compared to InSAR observations at the wet site (E2). Modified from Wendt (2024a).
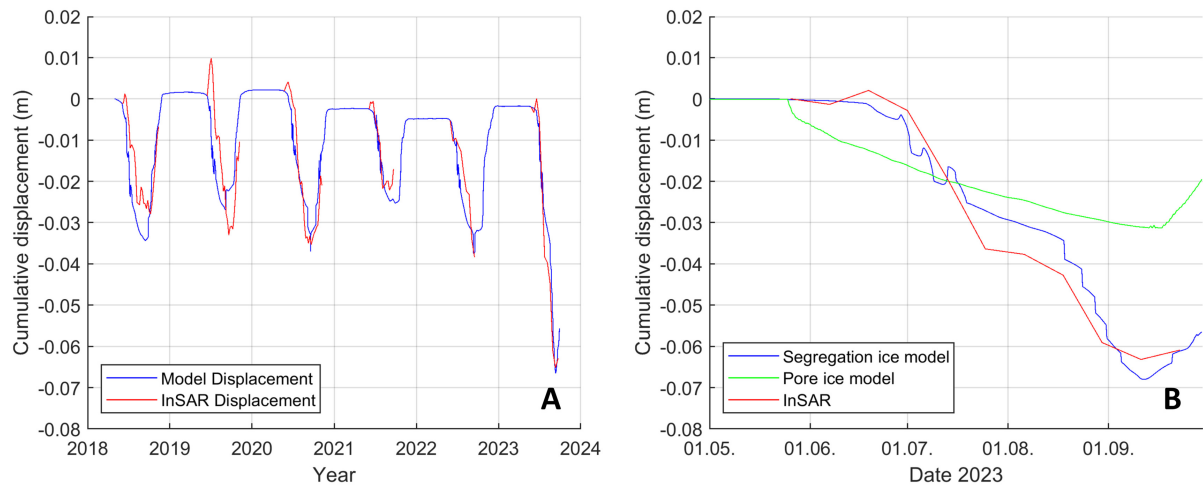
Figure 16: Simulations of segregation ice model. A. Simulated displacement time series compared to InSAR observations at the wet site (E10). B. Detailed view of the warm 2023 season, showing the difference between the two model configurations, compared to the InSAR observations. Modified from Wendt (2024).

6 Conclusions and prospects for future work

The *IceInSAR* pilot study confirms the ability of InSAR to infer information on the spatial and vertical variability of ground ice contents. While the pore-ice model set-up of the Permafrost_cci model is able to represent InSAR observations for dry conditions, it is clearly not able to represent the ground surface elevation dynamics for the selected wet site, due to the high sensitivity to excess ice. In this respect, InSAR time series can indirectly help improving the model results by documenting the variability of the ice content in the active layer and the uppermost permafrost. We conclude that InSAR has a clear potential for constraining the parametrization of the ground stratigraphy in future iterations of the Permafrost_cci model.

In the future, we see significant potential in improving Permafrost_cci ECV characterization in the following workflow steps:

- We need to develop realistic ingestion strategies avoiding computationally demanding workflows. InSAR clustering appears to be an appropriate solution to reduce the dimensionality of the InSAR products. The mean InSAR time series of each cluster may be used for assimilation. If it is still too computationally demanding, manually defined ground stratigraphy parameters associated to each cluster can be assimilated.

- Information provided by InSAR can be combined with landcover products used in the Permafrost_cci baseline model, or under development in the Permafrost_cci project (e.g. Option 6 outcome; Bartsch et al., 2024). We plan to develop composite InSAR–landcover products and test the impact on the model performance in selected regions. A natural first step in that direction is to systematically compare InSAR and landcover in several Arctic regions.

- InSAR processing workflows for large-scale processing at the pan-Arctic scale need to be developed. A growing number of InSAR Ground Motion Services (GMS) at the regional–continental scale are becoming operational (e.g. EGMS), but permafrost regions remain mostly undocumented. The research for GMS extension in the Arctic must intensify, as recommended by the Copernicus Polar Task Force (Duchossois et al., 2024).

These points are further discussed in the PVIR [RD-1].

7 References

7.1 Bibliography

Aga, J., Boike, J., Langer, M., Ingeman-Nielsen T., and Westermann S. (2023). Simulating ice segregation and thaw consolidation in permafrost environments with the CryoGrid community model. *The Cryosphere 17*(10), 4179–4206. https://doi.org/10.5194/tc-17-4179-2023.

Bartsch, A., Efimova, A., Widhalm, B., Muri, X., von Baeckmann, C., Bergstedt, H., Ermokhina, K., Hugelius, G., Heim, B., Leibmann, M., and Khairullin, R. (2024). Circumpolar Landcover Units (v1.1) [Data set]. Zenodo. https://doi.org/10.5281/zenodo.11486149.

Cable, S., Elberling B., and Kroon, A. (2018). Holocene permafrost history and cryostratigraphy in the High-Arctic Adventdalen Valley, central Svalbard. *Boreas* 47.2, 423–442. https://doi.org/10.1111/bor.12286.

Duchossois, G., Berdahl, M., Diehl, T., Garric, G., Humbert, A., Itkin, P., Jawak, S., and Tietsche, S. (2024). Copernicus polar roadmap for service evolution. Copernicus Polar Task Force. Publications Office of the European Union, Luxembourg. https://doi.org/10.2889/644108 .

Gilbert, G. L., O'Neill, H. B., Nemec, W., Thiel, C., Christiansen H. H., and Buylaert J.-P. (2018). Late Quaternary sedimentation and permafrost development in a Svalbard fjord-valley, Norwegian high Arctic. *Sedimentology* 65.7, pp. 2531–2558. https://doi.org/10.1111/sed.12476.

Härtel, S., and Christiansen H. H. (2014). *Geomorphological and Cryological map of Adventdalen, Svalbard*. https://doi.pangaea.de/10.1594/PANGAEA.833048.

Rasmussen, C. F., Christiansen, H. H. Buylaert, J.-P. Cunningham, A. Schneider, R. Knudsen M. F., and Stevens T. (2023). High-resolution OSL dating of loess in Adventdalen, Svalbard: Late Holocene dust activity and permafrost development. *Quaternary Science Reviews 310*, 108137. https://doi.org/10.1016/j.quascirev.2023.108137.

Rouyet, L., Strand, S. M., Christiansen, H. H., Lauknes T. R., and Larsen Y. (2019). Seasonal InSAR Displacements Documenting the Active Layer Freeze and Thaw Progression in Central-Western Spitsbergen, Svalbard. *Remote Sensing 13*(15), 2977. https://doi.org/10.3390/rs13152977.

Rouyet, L., Liu, L., Strand, S. M., Christiansen, H. H., Lauknes T. R., and Larsen Y. (2021). Seasonal InSAR Displacements Documenting the Active Layer Freeze and Thaw Progression in Central-Western Spitsbergen, Svalbard. *Remote Sensing 13*(15), 2977. https://doi.org/10.3390/rs13152977.

Rouyet, L., Bredal, M. B., Lauknes, T. R., Dehls, H. F., Larsen, Y., von Oostveen, J., Hindberg, H., and Wendt, L. (2024). InSAR Svalbard – User requirements, technical considerations, and product development plan. Report No. 2-2024, NORCE Energy and Technology. https://hdl.handle.net/11250/3125660.

Wendt, L. (2024a). Assessing ground ice changes in Svalbard from SAR interferometry and modelling. M.Sc. thesis. Department of Geoscience, Faculty of Mathematics and Natural Sciences, University of Oslo. http://hdl.handle.net/10852/112526.

Wendt, L. (2024b). Ground ice contents and InSAR displacements from Adventdalen, Svalbard. [Data set]. Zenodo. https://doi.org/10.5281/zenodo.11187360.

Westermann, S. et al. (2023). The CryoGrid community model (version 1.0) – a multi-physics toolbox for climate-driven simulations in the terrestrial cryosphere. *Geoscientific Model Development 16*(9), 2607–2647. https://doi.org/10.5194/gmd-16-2607-2023.

7.2 Acronyms

AD	Applicable Document
ADP	Algorithm Development Plan
ALT	Active Layer Thickness
ATBD	Algorithm Theoretical Basis Document
B.GEOS	B.Geos GmbH
CAR	Climate Assessment Report
CCI	Climate Change Initiative
CRDP	Climate Research Data Package
ECV	Essential Climate Variable
EO	Earth Observation
ESA	European Space Agency
E3UB	End-To-End ECV Uncertainty Budget
GAMMA	Gamma Remote Sensing AG
GCOS	Global Climate Observing System
GMS	Ground Motion Service
GT	Ground Temperature
GTN-P	Global Terrestrial Network for Permafrost
UIO	University of Oslo
INSAR	Synthetic Aperture Radar Interferometry
IPA	International Permafrost Association
NORCE	Norwegian Research Centre AS
PE	Permafrost Extent
PF	Permafrost Fraction
PSD	Product Specification Document
PUG	Product User Guide
PVASR	Product Validation and Algorithm Selection Report
PVIR	Product Validation and Intercomparison Report
PVP	Product Validation Plan
RD	Reference Document
RMSE	Root Mean Square Error
SAR	Synthetic Aperture Radar
SD	Surface Displacement
SSD	System Specification Document
URD	Users Requirement Document
URq	User Requirement
WMO	World Meteorological Organisation